THE JOURNAL OF PHYSICAL CHEMISTRY C
A JOURNAL OF THE AMERICAN CHEMICAL SOCIETY

pubs.acs.org/JPCC
Article

Soft X-ray Emission Spectroscopy of Phosphorus Compounds for Energy Conversion and Storage

Romualdus Enggar Wibowo,* Raul Garcia-Diez, Marianne van der Merwe, Daniel Duarte-Ruiz, Yang Ha, Wanli Yang, Martin Prokop, Tomas Bystron, Regan G. Wilks, Caterina Cocchi, and Marcus Bär*

Cite This: J. Phys. Chem. C 2025, 129, 7659−7666

ABSTRACT: Phosphorus (P) is a ubiquitous component of materials for energy conversion and storage. Despite the effectiveness of soft X-ray emission spectroscopy (XES) to characterize these complex materials, XES studies of P-containing compounds are still largely missing. In this investigation, the electronic structure and XES signatures from the P $L_{2,3}$-edge are probed for nine solid-state P-containing compounds characterized by various oxidation states and chemical environments: $GaP^{(3-)}$, $InP^{(3-)}$, red-$P^{(0)}$, $H_3P^{(3+)}O_3$, $Na_2H_2P_2^{(4+)}O_6$, $H_3P^{(5+)}O_4$, $KH_2P^{(5+)}O_4$, $Na_2HP^{(5+)}O_4$, and $InP^{(5+)}O_4$. The XES spectrum of each material exhibits distinct spectral fingerprints, which provide a robust basis for the speciation of complex P-containing samples. Density functional theory calculations shed light on the electronic structure of selected materials and particularly on the effect of phosphorus−oxygen hybridization. This study provides a comprehensive understanding of P $L_{2,3}$ XES spectral fingerprints across a wide range of oxidation states and chemical environments. These data sets and insights pave the way for dedicated future work, such as *in situ* and *operando* investigations of P-containing compounds in energy-related applications, where speciation of P compounds is needed.

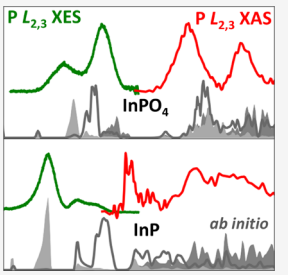

1. INTRODUCTION

Phosphorus (P) is a ubiquitous element in materials for energy conversion and storage. Phosphoric acid (H_3PO_4) serves as a proton conductor in high-temperature polymer electrolyte membrane fuel cells[1] and phosphoric acid fuel cells.[2] Solid acid fuel cells utilize CsH_2PO_4 as a solid electrolyte.[3] Phosphorus−carbon composites, such as those based on black phosphorus, graphite, and carbon nanotubes, along with metal phosphides like CoP, FeP, and CuP, have recently emerged as anodes for Na-ion and Li-ion batteries.[4−6] P-based materials such as triethyl phosphite (TEP), tributyl phosphate (TBP), and dimethyl methyl phosphonate (DMMP) have been used as electrolyte additives in the development of nonflammable Li-ion batteries.[7−10] P-containing compounds are also integral to photocatalysis technologies, with metal phosphides (e.g., InP and GaP),[11] elemental phosphorus (e.g., black phosphorus and red phosphorus),[12,13] and phosphate compounds (e.g., $Co_3(PO_4)_2$ and $FePO_4$)[11] playing key roles in photo- and cocatalysis for water splitting.[11] Finally, black phosphorus and GaInP-based materials have potential in photovoltaic applications.[14,15]

In recent years, tender X-ray absorption spectroscopy (XAS) at the P K-edge has been extensively used to study the electronic properties of various P-containing compounds and identify the presence of specific P-based groups, particularly phosphates (i.e., compounds containing $(P^{(5+)}O_4)^{3-}$ ion).[16−22] Besides P K-edge XAS, several XAS investigations of P compounds have also been conducted using soft X-rays at the P $L_{2,3}$-edge (also referred to as near-edge X-ray absorption fine structure spectroscopy, or NEXAFS).[23−28] For some P-containing compounds, such as organic P species, P $L_{2,3}$-edge XAS has been reported to provide distinct spectral features that aid in their characterization,[23,29] making it a valuable tool for the identification of a specific P species.

In addition to XAS, X-ray emission spectroscopy (XES) provides complementary insights into the electronic structure of materials. While XAS probes unoccupied states above the Fermi level (E_F), XES provides information on the occupied states below E_F. Soft XES at the P $L_{2,3}$-edge complements P $L_{2,3}$ XAS by probing active transitions from valence states with s and d characters. Similar to the P $L_{2,3}$ XAS, soft XES at the P $L_{2,3}$-edge has high surface sensitivity due to the low attenuation length of soft X-rays used to excite the P $L_{2,3}$ transition. This surface sensitivity makes P $L_{2,3}$ XES a powerful tool for investigating energy conversion and storage materials, such as photocatalysts or catalystlelectrolyte interfaces in fuel cells and electrolyzers, where surface properties are critical to chemical reactions. However, despite its potential, soft XES studies of P-containing compounds at the P $L_{2,3}$-edge remain extremely rare.

Received: December 20, 2024
Revised: February 25, 2025
Accepted: April 1, 2025
Published: April 10, 2025

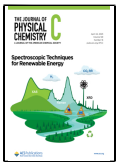

With this study, we aim to fill this gap by presenting and analyzing P $L_{2,3}$ XES measurements of nine solid-state P-containing compounds relevant for energy storage and conversion, covering a wide range of oxidation states (from 3− to 5+) and functional groups. The investigated compounds include $GaP^{(3-)}$, $InP^{(3-)}$, red-$P^{(0)}$, $H_3P^{(3+)}O_3$, $Na_2H_2P_2^{(4+)}O_6$, $H_3P^{(5+)}O_4$, $KH_2P^{(5+)}O_4$, $Na_2HP^{(5+)}O_4$, and $InP^{(5+)}O_4$. P $L_{2,3}$ XES spectra are recorded nonresonantly at excitation energies well above the P $L_{2,3}$-edge. To complement P $L_{2,3}$ XES data, P L_3 XES spectra are collected using photon energy slightly higher than the one of the P L_3 absorption edge but lower than the P L_2 absorption edge. In the analysis, the XES spectra are related to previously published XAS spectra at the P $L_{2,3}$-edge[28] (referred to as P $L_{2,3}$ XAS) and complemented by *ab initio* calculations of the projected density of states (pDOS) to better understand the electronic structure of the P compounds and thus interpret their XES spectral fingerprints. This study provides a comprehensive understanding of P $L_{2,3}$ XES spectral fingerprints for P-containing compounds across a wide range of oxidation states and chemical environments. These data sets and analyses are essential for future studies, for instance, *in situ* or *operando* investigations of P-containing compounds where the speciation of P-containing compounds is needed. This work aims at establishing P $L_{2,3}$ XES as a complementary method to P $L_{2,3}$ XAS measurements for the speciation of P compounds.

2. EXPERIMENTAL SECTION

2.1. Materials. In analogy with our previous XAS study,[28] materials probed in this work include gallium phosphide (GaP), indium phosphide (InP), red phosphorus (P, red phosphorus, ≥97.0%, Merck, hereafter referred to as "red-P"), phosphorus acid (crystalline H_3PO_3, 99%, Merck), disodium hypophosphate ($Na_2H_2P_2O_6{\cdot}10H_2O$, hereafter referred to as "$Na_2H_2P_2O_6$"), phosphoric acid (crystalline H_3PO_4, 99.99%, Merck), potassium hydrogen phosphate (KH_2PO_4, ≥99.0%, Mallinckrodt), sodium dihydrogen phosphate ($Na_2HPO_4{\cdot}12H_2O$, J.T. Baker, hereafter referred to as "Na_2HPO_4"), and indium phosphate ($InPO_4$, 98%, Alfa Aesar). Further details are provided in ref 28. All powder samples were finely ground using a clean mortar and pestle prior to the spectroscopic measurements. To prevent possible oxidation during grinding and mounting, these processes were conducted in an argon-purged glovebox.

2.2. X-ray Emission Spectroscopy (XES) and X-ray Absorption Spectroscopy (XAS) at the P $L_{2,3}$-Edge. *2.2.1. P $L_{2,3}$-Edge XES and XAS Measurement Procedure.* P $L_{2,3}$ XES measurements were performed in the iRIXS end-station, at beamline 8.0.1 of the Advanced Light Source (ALS),[30,31] Lawrence Berkeley National Laboratory. The experiments were carried out using the low-energy grating of the spherical grating monochromator of this undulator beamline. A high-throughput spectrometer equipped with a CCD (charge-coupled device) camera was employed to record the XES spectra. First, XES spectra were recorded as a function of excitation energies over the P $L_{2,3}$ absorption edge through a resonant inelastic X-ray scattering (RIXS) map. Experimental details on the RIXS maps are provided in Section S1.1 of the Supporting Information (SI). From the RIXS maps, the P $L_{2,3}$ (partial fluorescence yield, PFY) XAS of the P-containing compounds was determined by integrating the XES intensities arising from the P $L_{2,3}$-edge fluorescence (excluding elastic scattering contributions). Subsequently, the P L_3 absorption edge energy was determined from the P $L_{2,3}$ XAS inflection point. Details for PFY-XAS integration and L_3 absorption edge determination methods are provided in ref 28. Subsequently, P $L_{2,3}$ XES measurements were conducted at an excitation energy of 158 eV, at least 20 eV higher than the P L_3 absorption edge. To complement the P $L_{2,3}$ XES experiments, additional XES measurements were performed at an excitation energy slightly higher than the P L_3 absorption edge but lower than the P L_2 absorption edge to selectively excite the P L_3 edge (hereafter called P L_3 XES). The excitation energy for the P L_3 XES is unique for each P-containing compound, see Section S1.2, Table S2, and Figure S1 in the SI. The energy resolutions for the XES (both P $L_{2,3}$ XES and P L_3 XES) and P $L_{2,3}$ XAS measurements were approximately 0.16 and 0.17 eV, respectively. Detailed estimations of the energy resolution are provided in Section S1.3.

2.2.2. Energy Calibration and Further Data Treatment of the P $L_{2,3}$ XES and P $L_{2,3}$ XAS Spectra. To calibrate the excitation energy from the beamline, the P $L_{2,3}$ XAS spectrum of the InP sample was aligned to the corresponding XAS spectrum of InP reported in ref 32. Subsequently, the emission energy of the RIXS maps was calibrated using the elastic scattering feature, where the excitation energy equals the emission energy. Since both RIXS and XES measurements were recorded with the same spectrometer using a similar geometry, the same emission energy scale from the RIXS maps was used for both the P $L_{2,3}$ XES and the P L_3 XES data. Given that spectral contributions related to cosmic rays are also recorded during XES data collection, for accurate determination of the P $L_{2,3}$ and P L_3 XES spectra, these features are subtracted from the data. Furthermore, oxygen-containing P compounds (i.e., $H_3P^{(3+)}O_3$, $Na_2H_2P_2^{(4+)}O_6$, $H_3P^{(5+)}O_4$, $KH_2P^{(5+)}O_4$, $Na_2HP^{(5+)}O_4$, and $InP^{(5+)}O_4$) exhibit a spectral feature overlapping with the P $L_{2,3}$ XES data that is ascribed to the O K-edge emission excited by higher harmonics of the beamline and detected in the 4thorder of the spectrometer (referred to in this work as O K 4th XES). Therefore, for an accurate representation of the P $L_{2,3}$ and P L_3 XES spectra, the O K 4th XES is subtracted from the data. A detailed description of the procedure for the subtraction of cosmic rays and for the subtraction of the O K 4th XES-related spectral contributions is provided in Sections S2.1 and S2.2 and Figures S2−S4 of the SI. Finally, to enable an accurate comparison between P $L_{2,3}$ XAS spectra and pDOS calculations, a double arctan background representing the electronic transition from P 2p doublets into the continuum states was fitted and subtracted from the XAS, as reported in ref 28.

2.2.3. Electronic Band Gap Estimation from P L_3 XES and P $L_{2,3}$ XAS Spectra. For the approximation of the electronic band gap of P-containing compounds, the valence band maximum (VB_{max}) was estimated from the P L_3 XES data, while the conduction band minimum (CB_{min}) was derived from the P $L_{2,3}$ XAS data. The VB_{max} was approximated by linearly extrapolating the leading edge of the P L_3 XES data at high photon energies to the intersection with the linear fit of the spectral baseline. A similar procedure was conducted with the rising edge of P $L_{2,3}$ XAS data to estimate the CB_{min}. The electronic band gap was thus determined as the difference between the CB_{min} and the VB_{max}, i.e., $E_{gap} = CB_{min} - VB_{max}$. Further details and considerations, such as the considerations for using P L_3 XES spectra instead of P $L_{2,3}$ XES data for the

https://doi.org/10.1021/acs.jpcc.4c08618
J. Phys. Chem. C 2025, 129, 7659−7666

CB_{min} estimations, are provided in Section S2.3 and Figures S5−S7 of the SI.

2.3. Computational Details of the Ab Initio Calculations. The pDOS of red-P, InP, and $InPO_4$ was calculated using density functional theory (DFT) in the all-electron framework implemented in the "exciting" code.[33] The Perdew−Burke−Ernzerhof (PBE) implementation of the generalized gradient approximation for the exchange−correlation potential was employed in these calculations.[34] A plane-wave cutoff parameter of 8 was taken for red-P and InP, while for $InPO_4$, the value was reduced to 7. The following muffin-tin radii were used for the considered materials: 1.997 bohr for P in red phosphorus; 2.486 bohr for In and 2.099 bohr for P in InP; 2.580 bohr for In, 1.470 bohr for P, and 1.370 bohr for O in $InPO_4$. To sample the Brillouin zone, an 8 × 8 × 8 k-point grid was used for red-P, a 4 × 4 × 4 k-grid for $InPO_4$, and a 6 × 6 × 6 k-grid for InP. The input structures for red-P, $InPO_4$, and InP were taken from the Materials Project database[35] (entry nr. mp-157, mp-7566, and mp-20351, respectively) without performing any further optimization.

3. RESULTS AND DISCUSSION

The P $L_{2,3}$ XES and P $L_{2,3}$ XAS spectra of the P-containing compounds are presented in Figure 1. Hereafter, we focus primarily on the P $L_{2,3}$ XES data, as a detailed discussion of the P $L_{2,3}$ XAS is reported elsewhere.[28] As illustrated in the top panel of Figure 1, the phosphide compounds ($InP^{(3-)}$ and $GaP^{(3-)}$) display a strong emission line at a photon energy of around 120 eV (a''') followed by the weaker but broad emission feature (b''') around 124 eV. The same XES fingerprint was observed in previous P $L_{2,3}$ XES investigations of InP and GaP samples, attributing feature a''' mainly to P 3s states and b''' to both P 3s and P 3d states hybridized with either In 5s or Ga 4s states in InP or GaP, respectively.[32,36] Note that P 3p states are also present in the energy region of b'''.[36] However, due to the selection rule governing the P $L_{2,3}$ XES process, radiative decay of the P 2p core excited states can only occur via transitions from P 3s and 3d valence states to the P 2p core level, while transitions from P 3p to P 2p states are dipole-forbidden. Feature a''' in InP at 120.2 eV is slightly shifted to higher photon energy compared to GaP, where it appears at 119.7 eV. This is likely caused by the higher ionicity of InP compared to GaP.[36] Additionally, a very weak feature at ∼114 eV, marked by the symbol * in Figure 1, is observed in the spectrum of InP. A previous study suggests that it might arise from the hybridization of P 3s with In 4d states.[36]

The P $L_{2,3}$ XES spectrum of red-$P^{(0)}$ shows a broad shoulder around 118 eV labeled a'', followed by a strong XES feature b'' at 122 eV and a broad weaker feature c'' at 127 eV. The overall shape of this emission spectrum is highly comparable to the Si $L_{2,3}$ XES spectrum of elemental Si,[46−48] where the contribution of Si 3s states is present in both a'' and b''-like features, while Si 3d states manifest themselves in feature c''.[49,50] Similarly, in red-$P^{(0)}$, a'' and b'' can be mainly assigned to the P 3s states, while P 3d states are related to feature c''. Analogous to the P $L_{2,3}$ XES spectrum of InP and GaP discussed above, also, Si 3p states are present in the pDOS of Si, but the radiative transition into Si 2p states is dipole-forbidden in the Si $L_{2,3}$ XES.[51,52]

The oxygen-containing P compounds show distinct P $L_{2,3}$ XES spectral fingerprints. $Na_2HP^{(5+)}O_4$ and $InP^{(5+)}O_4$ display a broad emission feature a' at 120 eV and a stronger emission feature c' at 128 eV. The other oxygen-containing compounds,

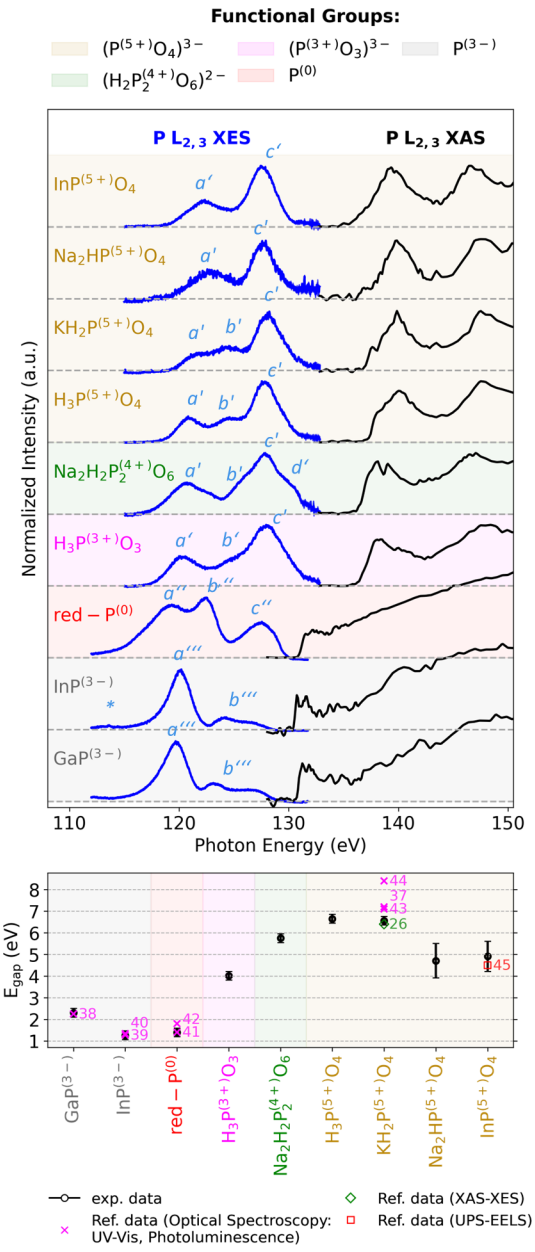

Figure 1. (Top) P $L_{2,3}$ XES and P $L_{2,3}$ XAS[28] of the investigated P compounds. For improved visualization, all spectra are normalized to zero at the baseline and unity at the maximum of the spectrum; additionally, the P $L_{2,3}$ XAS data of $GaP^{(3-)}$, $InP^{(3-)}$, and red-$P^{(0)}$ are magnified by a factor of 1.5. (Bottom) Electronic band gaps (E_{gap}) of P-containing compounds estimated from the P L_3 XES and P $L_{2,3}$ XAS spectra, compared to the reported band gaps that are available from the literature. Detailed values of the estimated E_{gap}, the respective uncertainties of the band gap, the values of the reported band gap referenced in this work (refs 26 and 37−45), and the methods used to determine the respective band gaps are provided in Table S3 of the SI.

$H_3P^{(3+)}O_3$, $Na_2H_2P_2{}^{(4+)}O_6$, $H_3P^{(5+)}O_4$, and $KH_2P^{(5+)}O_4$, exhibit more complex XES features. In all these spectra, there is a shoulder (b') at 126 eV, while $Na_2H_2P_2{}^{(4+)}O_6$ also exhibits another shoulder (d') at 130 eV. The P $L_{2,3}$ XES spectral fingerprints of the phosphates (functional group containing $(P^{(5+)}O_4)^{3-}$ ion) are very similar to the S $L_{2,3}$ XES of sulfate[53,54] (family of the $(S^{(6+)}O_4)^{2-}$ functional group), where the a' and c' features are commonly attributed to S 3s and 3d states, respectively.[53,54] This interpretation

https://doi.org/10.1021/acs.jpcc.4c08618
J. Phys. Chem. C 2025, 129, 7659−7666

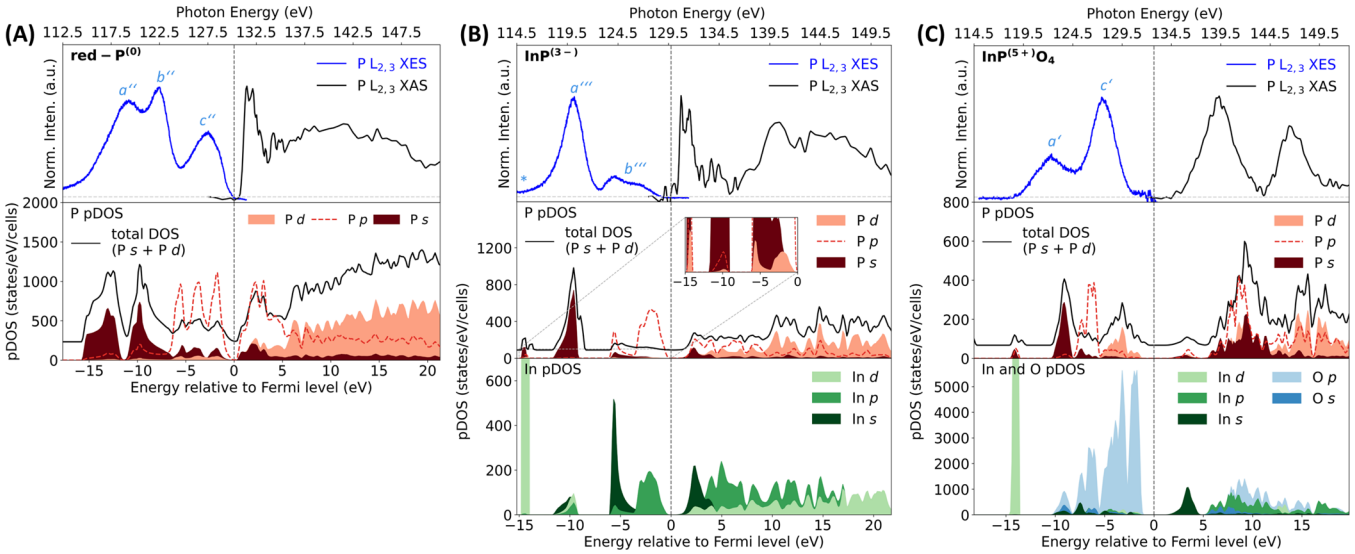

Figure 2. P $L_{2,3}$ XES, (background subtracted) P $L_{2,3}$ XAS spectra of P-containing compounds with (A) no ligand: red-$P^{(0)}$, (B) metallic ligand: $InP^{(3-)}$, and (C) oxygen ligand: $InP^{(5+)}O_4$ (top panels), as well as the respective *ab initio* calculated projected density of states (pDOS) of the P-containing compounds, including contributions from P states (center panels) and from the other elements (bottom panels). Contributions of P s, p, and d states are shown, while the "total DOS" (black line) is obtained as the sum of P s- and d-derived states only, which are targeted by transitions from P 2p core levels. Details for the total DOS summation are provided in the manuscript.

suggests that also in the considered P-based compounds, a' arises from P 3s states and c' from P 3d states. Additionally, high pDOS contributions from O 2p states are observed in the same energy region of c', indicating possible hybridization between O 2p and P 3d states. Beyond the emission features a' and c', the shoulder feature b' is interestingly only observed in oxygen-containing P compounds with two or more hydrogen (H) atoms. Considering that all compounds exhibiting feature b' have two bonds between P and OH (through the P−O−H bond), this observation suggests that feature b' may arise from the bonding environment between P atoms and their OH nearest neighbors. However, additional analysis is needed to ascertain this assessment. In contrast, the shoulder d' is observed only in $Na_2H_2P_2^{(4+)}O_6$. Interestingly, this feature is more pronounced in the P L_3 XES spectrum of $Na_2H_2P_2^{(4+)}O_6$ (see Figure S4B in the SI), indicating that feature d' may be related to resonant excitation processes. Further investigations are required to ultimately clarify the origin of this feature.

The electronic band gaps of each compound, derived from XES and XAS measurements, as reported in the bottom panel of Figure 1, can also be used to identify P-containing compounds. However, it is important to note that the CB_{min} estimated from XAS may be influenced by core−hole effects, potentially leading to an underestimation of the actual band gap, since the leading edge of the XAS spectrum's onset may correspond to a core exciton rather than to the true CB_{min}. This consideration might explain the relatively smaller band gap estimated here compared to the reference values that were reported for $KH_2P^{(5+)}O_4$ (see the bottom panel of Figure 1). Besides that, the herein-derived band gaps are in good agreement and are within uncertainties with the band gaps of the same P-containing compounds reported in the literature,[26,37−45] as detailed in Table S3, Section S2.3 of the SI.

In general, XES spectra exhibit distinct fingerprints at varying functional groups (e.g., phosphides vs phosphates), while more subtle differences can be observed within the same functional groups. Additionally, the peak positions of P $L_{2,3}$ XES data's most intense peak significantly shift for different functional groups, as seen from phosphides (feature a'''), to red-$P^{(0)}$ (feature b''), to the oxygen-containing P compounds (feature c'). It is interesting to note that subtle spectral differences and very small differences in peak positions were observed between the investigated oxygen-containing P compounds, such as phosphite ($H_3P^{(3+)}O_3$), hypophosphate ($Na_2H_2P_2^{(4+)}O_6$), and the phosphate compounds. This is likely attributed to a similar local environment around the P atoms, as all three groups of the oxygen-containing P compounds have at least three oxygen atoms in the first coordination shell, with no direct bonding between phosphorus and the associated metal cations. Similarly, the differences between phosphates are subtle since all investigated phosphates share the same coordination with four oxygen atoms around phosphorus, without direct metal−phosphorus bonding. However, although the difference is subtle, each oxygen-containing P compound exhibits unique spectral features, as demonstrated by the direct comparison example in Figure S9 in the SI. As such, even though fingerprinting of specific oxygen-containing P compounds is possible, careful analysis and observation are required, such as with the example given in Section S3 in the SI.

The unique spectral fingerprints and peak shifts identified in this study can serve as valuable tools for further P $L_{2,3}$ XES (*in situ* and *operando*) investigations of P-containing compounds where speciation is needed. For example, during the operation of high-temperature polymer electrolyte membrane fuel cells (HT-PEMFCs), the formation of P impurities such as $H_3P^{(3+)}O_3$ may occur at the Pt-catalyst|$H_3P^{(5+)}O_4$-electrolyte interface, which could also be followed by potential reoxidation of $H_3P^{(3+)}O_3$ to $H_3P^{(5+)}O_4$.[55−57] *Operando* P $L_{2,3}$ XES investigation could provide valuable insights into the nature of P species at the catalyst|electrolyte interface under operational conditions. Notably, the surface sensitivity of P $L_{2,3}$ transitions offers an advantage for such investigation at the interface, as also suggested in the previous *in situ* P K-edge XAS study of the Pt-catalyst|aq. $H_3P^{(3+)}O_3$-electrolyte

https://doi.org/10.1021/acs.jpcc.4c08618
J. Phys. Chem. C 2025, 129, 7659−7666

system.[58] For potential *operando* P $L_{2,3}$ XES investigations of P compounds in such a system, the data set presented in this study could facilitate the identification and characterization of P compounds. For instance, the data set presented in this study can be used as a reference spectrum for linear combination analysis (LCA) of a P $L_{2,3}$ XES spectrum recorded during *in situ* or *operando* investigation, enabling identification and quantification of species present under reaction conditions. An example of LCA application to identify and quantify species in an XES spectrum is reported elsewhere.[59]

To elucidate the influence of the functional groups on the electronic structure of the considered materials, the pDOS of three selected P-containing compounds with different chemical environments was calculated: (i) red-$P^{(0)}$ with no ligand, (ii) $InP^{(3-)}$ with a metallic ligand, and (iii) $InP^{(5+)}O_4$ with an oxygen ligand. The chosen materials enable a systematic comparison of P-containing compounds with increasing chemical complexity, ranging from a single element (red-$P^{(0)}$) to a binary ($InP^{(3-)}$) and ternary compound ($InP^{(5+)}O_4$). Notably, all three compounds share a common P core, and while both $InP^{(3-)}$ and $InP^{(5+)}O^4$ have the same cation (In), the local environment around P atoms varies between the two: metallic bonding in $InP^{(3-)}$ and covalent bonding with oxygen in $InP^{(5+)}O_4$.

Based on the atomic selection rules, prescribing that the electronic transitions involved in the P $L_{2,3}$ excitation process target P s and d states, in the analysis of the pDOS, we focus on these orbital contributions to complement the interpretation of the XES data. Specifically, we compare the P $L_{2,3}$ XES signal with the summed contributions of P s and d states in the pDOS, hereafter "total DOS" from the P $L_{2,3}$ transition. To determine this quantity, we first compute the P L_3 contribution (i.e., the density of states projected onto s, p, and d states of P, as shown in the center panel of Figure 2) and subsequently add the P L_2 contribution. The P L_2 pDOS contribution was determined by shifting the P L_3 pDOS by 0.7−1.0 eV, according to the doublet separation observed in the P $L_{2,3}$ XAS and in agreement with values reported in the NIST database.[60,61] Finally, the P L_2 intensity was estimated by multiplying the P L_3 pDOS with the relative occupancy of P L_2 to P L_3 (i.e., by 0.5).[53,62]

In Figure 2A, XAS and XES data for ligand-free red-$P^{(0)}$ are contrasted against pDOS results highlighting the P atomic orbital contributions. This comparison shows a good match between experimental and calculated data. In particular, we notice that features *a″* and *b″* arise mainly from P 3s states with some contribution from P 3d states observed in the XES feature *c″*. In Figure 2B, the same analysis is proposed for the $InP^{(3-)}$ containing a metallic ligand. Due to the coexistence of two atomic species in this compound, the pDOS analysis is performed for both P and In contributions. Similar to red-$P^{(0)}$, the main features in the XES spectrum can be assigned to P 3s states, while the contribution from P 3d states to feature *b′* is evident from the inset in the middle panel of Figure 2B. The pDOS analysis of the In orbitals (bottom panel of Figure 2B) reveals contributions from the In 5s-derived states to the XES feature *b′*, as well as from In 4d orbitals to the weak peak marked as * in Figure 1, in agreement with previous studies.[32,36] Similar to red-$P^{(0)}$, there is a good match between the experimental P $L_{2,3}$ XES and the total pDOS derived from P s and dstates. It is worth emphasizing that the total DOS reported in Figure 2 represents only the target states available for the excited core electrons, with no core−hole effects being accounted for. As such, it is unsurprising that agreement with the experimental P $L_{2,3}$ XAS data is inferior compared to spectra computed from the solution of the Bethe−Salpeter equation reported in ref 28. Nevertheless, the total DOS still provides a qualitatively reliable mapping for the spectral features observed in both the P $L_{2,3}$ XES and P $L_{2,3}$ XAS data.

For $InP^{(5+)}O_4$, the P 3s and P 3d states contribute to features *a′* and *c′*, respectively, see top and center panels of Figure 2C. The strong contribution from O 2p states and some contributions from In 5s and In 5p states in the energy region of feature *c′* can be seen in the bottom panel of Figure 2C. However, the match between the experimental P $L_{2,3}$ XES and the total DOS obtained from the summed contribution from P s and d states seems to be inferior to the respective comparison for red-$P^{(0)}$ and $InP^{(3-)}$. This finding is a signature of the more complex chemical environment of this ternary material, where, as expected, interspecies hybridization plays a role not only in determining the electronic structure of the material but also in the selection rules for the electronic transitions contributing to the XES. Notably, hybridization is expected in materials with highly electronegative ligands, such as oxygen. It should be stressed that the pDOS provides only the amount of states available in a certain energy window but does not entail any quantitative information about the transition probabilities. Hence, it is expected that in simpler materials like red-$P^{(0)}$ and $InP^{(3-)}$, XES spectral features can be better described by the pDOS compared to more complex compounds, where it is legitimate to expect that wavefunction mixing primarily due to hybridization, see Figure S10, becomes more prominent and makes the comparison of experimental data with pDOS less straightforward.

4. SUMMARY AND CONCLUSIONS

P $L_{2,3}$ XES experiments were carried out on a set of nine P-containing compounds covering a wide range of oxidation states and chemical environments. Our results reveal the primary role of functional groups in determining the spectral fingerprints of the materials and the impact of oxidation on spectral shifts. A careful analysis of P L_3 XES and P $L_{2,3}$ XAS data enables the estimation of the electronic band gaps of the considered P-containing compounds, which also provide material-specific indications useful for speciation. A comparison of experimental XES data with calculated pDOS revealed that XES spectra of P compounds without ligands (e.g., elemental red-P) and with metallic ligands mainly arise from the transition to P s and d-derived states, while in ternary P compounds with oxygen ligands, hybridization increases the complexity of the electronic structure, rendering the comparison with experimental data less straightforward. Nonetheless, the pDOS analysis provides valuable insights for the interpretation of the XES data.

This study highlights the importance of soft XES at the P $L_{2,3}$-edge as a powerful tool for identifying P-containing compounds and investigating their electronic structure, integrating the information provided by P $L_{2,3}$ XAS. As such, the comprehensive P $L_{2,3}$ XES spectral data sets and analyses presented in this study serve as valuable references for the identification of P-containing compounds in future investigations. These data sets are particularly relevant for *in situ* or *operando* P $L_{2,3}$ XES studies of P compounds for energy conversion and storage applications, where they can facilitate the speciation of materials that are formed during the reaction,

https://doi.org/10.1021/acs.jpcc.4c08618
J. Phys. Chem. C 2025, 129, 7659−7666

using approaches such as spectral fingerprinting or linear combination analysis.

■ ASSOCIATED CONTENT

Data Availability Statement

The data presented in this work are available in the ZENODO repository at the following links: 10.5281/zenodo.13983118 for the experimental data set and 10.5281/zenodo.7839832 for the computational data.

Supporting Information

The Supporting Information is available free of charge at https://pubs.acs.org/doi/10.1021/acs.jpcc.4c08618.

> Further experimental details for the P $L_{2,3}$-edge RIXS, P $L_{2,3}$ XES, P L_3 XES, and P $L_{2,3}$ XAS; estimation of the energy resolution for the P $L_{2,3}$ XES; further details on P $L_{2,3}$ XES and P L_3 XES data analysis, including subtraction of cosmic ray from the XES data set, subtraction of O K 4th XES from P $L_{2,3}$ XES and P L_3 XES, electronic band gap estimation process and further considerations for the approximation process, and alignment method of *ab initio* calculated pDOS with XAS and XES spectra; overlap between the pDOS of P p-derived states and the pDOS of other orbitals of the non-P atoms (PDF)

■ AUTHOR INFORMATION

Corresponding Authors

Romualdus Enggar Wibowo − *Department of Interface Design, Helmholtz-Zentrum Berlin für Materialien und Energie GmbH (HZB), Berlin 12489, Germany;* Present Address: Young Investigator Group Electrochemical Conversion of CO_2, Helmholtz-Zentrum Berlin für Materialien and Energie GmbH (HZB), Hahn-Meitner-Platz 1, 14109 Berlin, Germany; orcid.org/0000-0002-8325-0413; Email: enggar.wibowo@helmholtz-berlin.de

Marcus Bär − *Department of Interface Design, Helmholtz-Zentrum Berlin für Materialien und Energie GmbH (HZB), Berlin 12489, Germany; Energy Materials In-situ Laboratory Berlin (EMIL), HZB, Berlin 12489, Germany; Department of Chemistry and Pharmacy, Friedrich-Alexander-Universität Erlangen-Nürnberg, Erlangen 91058, Germany; Department of X-ray Spectroscopy at Interfaces of Thin Films, Helmholtz Institute Erlangen-Nürnberg for Renewable Energy (HI ERN), Berlin 12489, Germany;* orcid.org/0000-0001-8581-0691; Email: marcus.baer@helmholtz-berlin.de

Authors

Raul Garcia-Diez − *Department of Interface Design, Helmholtz-Zentrum Berlin für Materialien und Energie GmbH (HZB), Berlin 12489, Germany;* orcid.org/0009-0000-9374-1083

Marianne van der Merwe − *Department of Interface Design, Helmholtz-Zentrum Berlin für Materialien und Energie GmbH (HZB), Berlin 12489, Germany;* orcid.org/0000-0002-3182-1392

Daniel Duarte-Ruiz − *Institute of Physics, Carl von Ossietzky Universität Oldenburg, Oldenburg 26129, Germany;* orcid.org/0000-0003-2424-1397

Yang Ha − *Advanced Light Source (ALS), Lawrence Berkeley National Laboratory, Berkeley, California 94720, United States;* orcid.org/0000-0001-5684-8420

Wanli Yang − *Advanced Light Source (ALS), Lawrence Berkeley National Laboratory, Berkeley, California 94720, United States;* orcid.org/0000-0003-0666-8063

Martin Prokop − *Department of Inorganic Technology, University of Chemistry and Technology Prague, Prague 6 166 28, Czech Republic*

Tomas Bystron − *Department of Inorganic Technology, University of Chemistry and Technology Prague, Prague 6 166 28, Czech Republic*

Regan G. Wilks − *Department of Interface Design, Helmholtz-Zentrum Berlin für Materialien und Energie GmbH (HZB), Berlin 12489, Germany; Energy Materials In-situ Laboratory Berlin (EMIL), HZB, Berlin 12489, Germany;* orcid.org/0000-0001-5822-8399

Caterina Cocchi − *Institute of Physics, Carl von Ossietzky Universität Oldenburg, Oldenburg 26129, Germany;* orcid.org/0000-0002-9243-9461

Complete contact information is available at: https://pubs.acs.org/10.1021/acs.jpcc.4c08618

Author Contributions

R.E.W. carried out the XES measurements together with M.v.d.M, R.G.-D., R.G.W., and M.B. W.Y. provided support for the XES measurement at the BL8.0.1. The *ab initio* calculations and their analysis were carried out by D.D.-R. and C.C. Additional XES measurements of all P-containing compounds were conducted by Y.H. with the support from W.Y., for measures of reproducibility. M.P. synthesized the $Na_2H_2P_2^{(4+)}O_6$ used in this study. Data analysis and drafting of the original manuscript were carried out by R.E.W. with insightful advice from M.v.d.M., R.G.-D., T.B., R.G.W., C.C., and M.B. Acquisitions of the funding necessary for this project were carried out by M.B. All authors provided constructive advice on the manuscript and have given approval to its final version.

Notes

The authors declare no competing financial interest.

■ ACKNOWLEDGMENTS

Romualdus Enggar Wibowo is grateful for the funding from the Deutsche Forschungsgemeinschaft: DFG OPERACELL [BA 2900/9-1], for the OperaCell Project. Raul Garcia-Diez acknowledges funding by the German Federal Ministry of Education and Research in the framework of the CatLab project (03EW0015A/B). Daniel Duarte-Ruiz and Caterina Cocchi acknowledge financial support from the German Ministry for Education and Research (BMBF), project number 03XP0328A and Professorinnenprogramm III, and computational resources from the high-performance computing cluster CARL at the University of Oldenburg, funded by the German Research Foundation (project no. INST 184/157-1 FUGG) and by the Ministry of Science and Culture of the Lower Saxony State. Martin Prokop and Tomas Bystron acknowledge funding by the Czech Science Foundation (GAČR) through project no. 22-23668K and by the project Energy Conversion and Storage, funded as project no. CZ.02.01.01/00/22_008/0004617 by Programme Johannes Amos Comenius, called Excellent Research. The authors thank Prof. Dr. Karel Bouzek, from the Dept. of Inorganic Technology of UCT Prague, for his support in the OperaCell Project. The authors thank the ALS for the access to synchrotron radiation beamtime for this investigation. This research used resources of the Advanced

Light Source (ALS), which is a DOE Office of Science User Facility under contract no. DE-AC02-05CH11231. All of the graphs presented in this work were plotted with a Python script built on the Matplotlib package.[63]

REFERENCES

(1) Araya, S. S.; Zhou, F.; Liso, V.; Sahlin, S. L.; Vang, J. R.; Thomas, S.; Gao, X.; Jeppesen, C.; Kær, S. K. A Comprehensive Review of PBI-Based High Temperature PEM Fuel Cells. *Int. J. Hydrog. Energy* **2016**, *41* (46), 21310−21344.
(2) Sammes, N.; Bove, R.; Stahl, K. Phosphoric Acid Fuel Cells: Fundamentals and Applications. *Curr. Opin. Solid State Mater. Sci.* **2004**, *8* (5), 372−378.
(3) Qing, G.; Kikuchi, R.; Takagaki, A.; Sugawara, T.; Oyama, S. T. $CsH_5(PO_4)_2$ Doped Glass Membranes for Intermediate Temperature Fuel Cells. *J. Power Sources* **2014**, *272*, 1018−1029.
(4) Liu, W.; Zhi, H.; Yu, X. Recent Progress in Phosphorus Based Anode Materials for Lithium/Sodium Ion Batteries. *Energy Storage Materials* **2019**, *16*, 290−322.
(5) Jin, H.; Zhang, T.; Chuang, C.; Lu, Y.-R.; Chan, T.-S.; Du, Z.; Ji, H.; Wan, L. Synergy of Black Phosphorus−Graphite−Polyaniline-Based Ternary Composites for Stable High Reversible Capacity Na-Ion Battery Anodes. *ACS Appl. Mater. Interfaces* **2019**, *11* (18), 16656−16661.
(6) Li, M.; Li, W.; Hu, Y.; Yakovenko, A. A.; Ren, Y.; Luo, J.; Holden, W. M.; Sun, X.; et al. New Insights into the High-Performance Black Phosphorus Anode for Lithium-Ion Batteries. *Adv. Mater.* **2021**, *33* (35), 2101259.
(7) Li, C.; Wu, S.; Qiu, Y.; Lu, D. Phosphorus-Containing $C_{12}H_{27}O_4P$ as Functional Electrolyte Additives for High-Voltage $LiNi_{0.5}Mn_{1.5}O_4$/Graphite Li-Ion Batteries with Excellent Electrochemical Performance. *Adv. Mater. Intefaces* **2021**, *8* (3), 2001588.
(8) Tu, W.; Xia, P.; Zheng, X.; Ye, C.; Xu, M.; Li, W. Insight into the Interaction between Layered Lithium-Rich Oxide and Additive-Containing Electrolyte. *J. Power Sources* **2017**, *341*, 348−356.
(9) Boorboor Ajdari, F.; Fathollahi Zonouz, A.; Heydari, A.; Shokoui Mehrabani, H.; Shakourian-Fard, M.; Kamath, G.; Ghasemi, F.; Kahrizi, M. Exploring the Effects of Dopamine and DMMP Additives on Improving the Cycle Boosting and Nonflammability of Electrolytes in Full-Cell Lithium-Ion Batteries (18650). *J. Phys. Chem. C* **2023**, *127* (17), 8195−8207.
(10) Bolloju, S.; Vangapally, N.; Elias, Y.; Luski, S.; Wu, N.-L.; Aurbach, D. Electrolyte Additives for Li-Ion Batteries: Classification by Elements. *Prog. Mater. Sci.* **2025**, *147*, No. 101349.
(11) Hu, Z.; Shen, Z.; Yu, J. C. Phosphorus Containing Materials for Photocatalytic Hydrogen Evolution. *Green Chem.* **2017**, *19* (3), 588−613.
(12) Shen, Z.-K.; Yuan, Y.-J.; Pei, L.; Yu, Z.-T.; Zou, Z. Black Phosphorus Photocatalysts for Photocatalytic H2 Generation: A Review. *Chemical Engineering Journal* **2020**, *386*, No. 123997.
(13) Fung, C.-M.; Er, C.-C.; Tan, L.-L.; Mohamed, A. R.; Chai, S.-P. Red Phosphorus: An Up-and-Coming Photocatalyst on the Horizon for Sustainable Energy Development and Environmental Remediation. *Chem. Rev.* **2022**, *122* (3), 3879−3965.
(14) Geisz, J. F.; Steiner, M. A.; García, I.; Kurtz, S. R.; Friedman, D. J. Enhanced External Radiative Efficiency for 20.8% Efficient Single-Junction GaInP Solar Cells. *Appl. Phys. Lett.* **2013**, *103* (4), No. 041118.
(15) Batmunkh, M.; Bat-Erdene, M.; Shapter, J. G. Black Phosphorus: Synthesis and Application for Solar Cells. *Adv. Energy Mater.* **2018**, *8* (5), 1701832.
(16) Ajiboye, B.; Akinremi, O. O.; Jürgensen, A. Experimental Validation of Quantitative XANES Analysis for Phosphorus Speciation. *Soil Sci. Soc. Am. j.* **2007**, *71* (4), 1288−1291.
(17) Ajiboye, B.; Akinremi, O. O.; Hu, Y.; Flaten, D. N. Phosphorus Speciation of Sequential Extracts of Organic Amendments Using Nuclear Magnetic Resonance and X-ray Absorption Near-Edge Structure Spectroscopies. *J. environ. qual.* **2007**, *36* (6), 1563−1576.
(18) Kruse, J.; Leinweber, P. Phosphorus in Sequentially Extracted Fen Peat Soils: A K-Edge X-Ray Absorption near-Edge Structure (XANES) Spectroscopy Study. *J. Plant Nutr. Soil Sci.* **2008**, *171* (4), 613−620.
(19) Kruse, J.; Negassa, W.; Appathurai, N.; Zuin, L.; Leinweber, P. Phosphorus Speciation in Sequentially Extracted Agro-Industrial By-Products: Evidence from X-ray Absorption Near Edge Structure Spectroscopy. *J. environ. qual.* **2010**, *39* (6), 2179−2184.
(20) Luo, L.; Ma, Y.; Sanders, R. L.; Xu, C.; Li, J.; Myneni, S. C. B. Phosphorus Speciation and Transformation in Long-Term Fertilized Soil: Evidence from Chemical Fractionation and P K-Edge XANES Spectroscopy. *Nutr Cycl Agroecosyst* **2017**, *107* (2), 215−226.
(21) Vogel, C.; Rivard, C.; Wilken, V.; Muskolus, A.; Adam, C. Performance of Secondary P-Fertilizers in Pot Experiments Analyzed by Phosphorus X-Ray Absorption near-Edge Structure (XANES) Spectroscopy. *Ambio* **2018**, *47* (S1), 62−72.
(22) Babos, D. V.; Castro, J. P.; Andrade, D. F.; Costa, V. C.; Pereira-Filho, E. R. Determination and Speciation of Phosphorus in Fertilizers and Mineral Supplements for Cattle by X-Ray Absorption near-Edge Structure Spectroscopy: A Simple Nondestructive Method. *Anal. Methods* **2019**, *11* (11), 1508−1515.
(23) Kruse, J.; Leinweber, P.; Eckhardt, K.-U.; Godlinski, F.; Hu, Y.; Zuin, L. Phosphorus $L_{2,3}$-Edge XANES: Overview of Reference Compounds. *J. Synchrotron Rad* **2009**, *16* (2), 247−259.
(24) Nicholls, M. A.; Bancroft, G. M.; Norton, P. R.; Kasrai, M.; De Stasio, G.; Frazer, B. H.; Wiese, L. M. Chemomechanical Properties of Antiwear Films Using X-Ray Absorption Microscopy and Nano-indentation Techniques. *Tribol. Lett.* **2004**, *17* (2), 245−259.
(25) Yin, Z.; Kasrai, M.; Fuller, M.; Bancroft, G. M.; Fyfe, K.; Tan, K. H. Application of Soft X-Ray Absorption Spectroscopy in Chemical Characterization of Antiwear Films Generated by ZDDP Part I: The Effects of Physical Parameters. *Wear* **1997**, *202* (2), 172−191.
(26) Kucheyev, S. O.; Bostedt, C.; van Buuren, T.; Willey, T. M.; Land, T. A.; Terminello, L. J.; Felter, T. E.; Hamza, A. V.; Demos, S. G.; Nelson, A. J. Electronic Structure of $KD_{2x}H_{2(1-x)}PO_4$ Studied by Soft x-Ray Absorption and Emission Spectroscopies. *Phys. Rev. B* **2004**, *70* (24), No. 245106.
(27) Li, X.; Liu, B.; Yan, C.; Liu, C.; Ju, X. Investigating the Surface Electronic Structures of Retired Components and Irradiated KDP Crystals with Different Fluences by XANES Spectroscopy. *Opt. Mater. Express* **2018**, *8* (4), 816.
(28) Wibowo, R. E.; Garcia-Diez, R.; van der Merwe, M.; Bär, M.; et al. Core-Level Spectroscopy with Hard and Soft X-Rays on Phosphorus-Containing Compounds for Energy Conversion and Storage. *J. Phys. Chem. C* **2023**, *127* (42), 20582−20593.
(29) Li, Y.-R.; Pereira, G.; Kasrai, M.; Norton, P. R. The Effect of Steel Hardness on the Performance of ZDDP Antiwear Films: A Multi-Technique Approach. *Tribol Lett.* **2008**, *29* (3), 201−211.
(30) Qiao, R.; Li, Q.; Zhuo, Z.; Sallis, S.; Fuchs, O.; Blum, M.; Weinhardt, L.; Heske, C.; Yang, W.; et al. High-Efficiency *in Situ* Resonant Inelastic x-Ray Scattering (IRIXS) Endstation at the Advanced Light Source. *Rev. Sci. Instrum.* **2017**, *88* (3), No. 033106.
(31) Jia, J. J.; Callcott, T. A.; Yurkas, J.; Ellis, A. W.; Himpsel, F. J.; Samant, M. G.; Stöhr, J.; Ederer, D. L.; Carlisle, J. A.; Hudson, E. A.; Terminello, L. J.; Shuh, D. K.; Perera, R. C. C. First Experimental Results from IBM/TENN/TULANE/LLNL/LBL Undulator Beamline at the Advanced Light Source. *Rev. Sci. Instrum.* **1995**, *66* (2), 1394−1397.
(32) Domashevskaya, E. P.; Kashkarov, V. M.; Seredin, P. V.; Terekhov, V. A.; Turishchev, S. Yu.; Arsentyev, I. N.; Ulin, V. P. Investigation of Porous InP by X-Ray Diffraction, IR Spectroscopy, USXES, XANES Spectroscopy, and Photoluminescence. *Bull. Russ. Acad. Sci. Phys.* **2008**, *72* (4), 439−442.
(33) Gulans, A.; Kontur, S.; Meisenbichler, C.; Nabok, D.; Pavone, P.; Rigamonti, S.; Sagmeister, S.; Werner, U.; Draxl, C. Exciting: A Full-Potential All-Electron Package Implementing Density-Functional Theory and Many-Body Perturbation Theory. *J. Phys.: Condens. Matter* **2014**, *26* (36), No. 363202.

https://doi.org/10.1021/acs.jpcc.4c08618
J. Phys. Chem. C 2025, 129, 7659−7666

(34) Perdew, J. P.; Burke, K.; Ernzerhof, M. Generalized Gradient Approximation Made Simple. *Phys. Rev. Lett.* **1996**, *77* (18), 3865−3868.
(35) Jain, A.; Ong, S. P.; Hautier, G.; Chen, W.; Richards, W. D.; Dacek, S.; Cholia, S.; Gunter, D.; Skinner, D.; Ceder, G.; Persson, K. A. Commentary: The Materials Project: A Materials Genome Approach to Accelerating Materials Innovation. *APL Materials* **2013**, *1* (1), No. 011002.
(36) Lin, L.; Woods, G. T.; Callcott, T. A. Soft-x-Ray Fluorescence Spectra of III-V Phosphides BP, GaP, and InP. *Phys. Rev. B* **2001**, *63* (23), No. 235107.
(37) Liu, C. S.; Kioussis, N.; Demos, S. G.; Radousky, H. B. Electron- or Hole-Assisted Reactions of H Defects in Hydrogen-Bonded KDP. *Phys. Rev. Lett.* **2003**, *91* (1), No. 015505.
(38) Lorenz, M. R.; Pettit, G. D.; Taylor, R. C. Band Gap of Gallium Phosphide from 0 to 900°K and Light Emission from Diodes at High Temperatures. *Phys. Rev.* **1968**, *171* (3), 876−881.
(39) Kittel, C. *Introduction to Solid State Physics*, 8th ed.; Wiley-VCH: 2004.
(40) Zafar, F.; Iqbal, A. Indium Phosphide Nanowires and Their Applications in Optoelectronic Devices. *Proceedings of the Royal Society A: Mathematical, Physical and Engineering Sciences* **2016**, *472* (2187), 20150804.
(41) Ansari, S. A.; Khan, Z.; Ansari, M. O.; Cho, M. H. Earth-Abundant Stable Elemental Semiconductor Red Phosphorus-Based Hybrids for Environmental Remediation and Energy Storage Applications. *RSC Adv.* **2016**, *6* (50), 44616−44629.
(42) Xuan, Y.; Quan, H.; Shen, Z.; Zhang, C.; Yang, X.; Lou, L. L.; Liu, S.; Yu, K. Band-Gap and Charge Transfer Engineering in Red Phosphorus-Based Composites for Enhanced Visible-Light-Driven H_2 Evolution. *Chem. - Eur. J.* **2020**, *26* (10), 2285−2292.
(43) Lin, Z.; Wang, Z.; Chen, C.; Lee, M.-H. Mechanism of Linear and Nonlinear Optical Effects of KDP and Urea Crystals. *J. Chem. Phys.* **2003**, *118* (5), 2349−2356.
(44) Carrs, C. W.; Radousky, H. B.; Rubenchik, A. M.; Feit, M. D.; Demos, S. G. Localized Dynamics during Laser-Induced Damage in Optical Materials. *Phys. Rev. Lett.* **2004**, *92* (8), No. 087401.
(45) Wager, J. F.; Wilmsen, C. W.; Kazmerski, L. L. Estimation of the Band Gap of InPO4. *Appl. Phys. Lett.* **1983**, *42* (7), 589−591.
(46) Iwami, M.; Hirai, M.; Kusaka, M.; Kubota, M.; Yamamoto, S.; Nakamura, H.; Watabe, H.; Kawai, M.; Soezima, H. Construction of a Soft X-Ray Emission Spectroscopy (SXES) Apparatus and Its Application for Study of Electronic and Atomic Structures of a Multilayer System. *Jpn. J. Appl. Phys.* **1990**, *29*, 1353.
(47) Kurmaev, E. Z.; Fedorenko, V. V.; Shamin, S. N.; Postnikov, A. V.; Wiech, G.; Kim, Y. Small-Spot X-Ray Emission Spectroscopy and Its Application for Study of Electronic Structure and Chemical Bonding in Solids. *Phys. Scr.* **1992**, *1992* (T41), 288.
(48) Shulakov, A. S.; Braiko, A. P.; Bukin, S. V.; Drozd, V. E. X-Ray Spectral Analysis of the Interface of a Thin Al_2O_3 Film Prepared on Silicon by Atomic Layer Deposition. *Phys. Solid State* **2004**, *46* (6), 1145−1148.
(49) Manyakin, M. D.; Kurganskii, S. I. Electronic Structure of Stishovite SiO_2. *J. Phys.: Conf. Ser.* **2019**, *1352* (1), No. 012032.
(50) Simunek, A.; Vackar, J.; Wiech, G. Local s, p and d Charge Distributions and X-Ray Emission Bands of SiO2: Alpha -Quartz and Stishovite. *J. Phys.: Condens. Matter* **1993**, *5* (7), 867.
(51) Gritsenko, V. A.; Novikov, Yu. N.; Shaposhnikov, A. V.; Morokov, Yu. N. Numerical Simulation of Intrinsic Defects in SiO_2 and Si_3N_4. *Semiconductors* **2001**, *35* (9), 997−1005.
(52) Wiech, G.; Kurmaev, E. Z. X-Ray Emission Bands and Electronic Structure of Crystalline and Vitreous Silica (SiO_2). *J. Phys. C: Solid State Phys.* **1985**, *18* (22), 4393.
(53) Weinhardt, L.; Hauschild, D.; Steininger, R.; Jiang, N.; Blum, M.; Yang, W.; Heske, C. Sulfate Speciation Analysis Using Soft X-Ray Emission Spectroscopy. *Anal. Chem.* **2021**, *93* (23), 8300−8308.
(54) Duncan, D. A.; Kephart, J. M.; Horsley, K.; Blum, M.; Heske, C.; et al. Characterization of Sulfur Bonding in CdS:O Buffer Layers for CdTe-Based Thin-Film Solar Cells. *ACS Appl. Mater. Interfaces* **2015**, *7* (30), 16382−16386.
(55) Prokop, M.; Bystron, T.; Bouzek, K. Electrochemistry of Phosphorous and Hypophosphorous Acid on a Pt Electrode. *Electrochim. Acta* **2015**, *160*, 214−218.
(56) Prokop, M.; Bystron, T.; Paidar, M.; Bouzek, K. H_3PO_3 Electrochemical Behaviour on a Bulk Pt Electrode: Adsorption and Oxidation Kinetics. *Electrochim. Acta* **2016**, *212*, 465−472.
(57) Wibowo, R. E.; Garcia-Diez, R.; Bystron, T.; Bär, M.; et al. Oxidation of Aqueous Phosphorous acid Electrolyte in Contact with Pt Studied by X-Ray Photoemission Spectroscopy. *ACS Appl. Mater. Interfaces* **2023**, *15* (44), 51989−51999.
(58) Wibowo, R. E.; Garcia-Diez, R.; Bystron, T.; Bär, M.et al.Elucidating the Complex Oxidation Behavior of Aqueous H_3PO_3 on Pt Electrodes via In Situ Tender X-Ray Absorption Near-Edge Structure Spectroscopy at the P K-Edge. *J. Am. Chem. Soc.* **2024**. *1467386*.
(59) Léon, A.; Fiedler, A.; Blum, M.; Yang, W.; Bär, M.; Scheiba, F.; Ehrenberg, H.; Heske, C.; Weinhardt, L. Electrolyte Stability and Discharge Products of an Ionic-Liquid-Based Li−O_2 Battery Revealed by Soft X-Ray Emission Spectroscopy. *J. Phys. Chem. C* **2019**, *123* (51), 30827−30832.
(60) Dudzik, E.; Müller, C.; McGovern, I. T.; Lloyd, D. R.; Patchett, A.; Zahn, D. R. T.; Johal, T.; McGrath, R. H_2S Adsorption on the (110) Surfaces of III−V Semiconductors. *Surf. Sci.* **1995**, *344* (1−2), 1−10.
(61) Poirier, D. M.; Weaver, J. H. InP(110) by XPS. *Surf. Sci. Spectra* **1993**, *2* (3), 256−262.
(62) Weinhardt, L.; Hauschild, D.; Fuchs, O.; Steininger, R.; Jiang, N.; Blum, M.; Heske, C.; et al. Satellite-Dominated Sulfur $L_{2,3}$ X-Ray Emission of Alkaline Earth Metal Sulfides. *ACS Omega* **2023**, *8* (5), 4921−4927.
(63) Hunter, J. D. Matplotlib: A 2D Graphics Environment. *Comput. Sci. Eng.* **2007**, *9* (3), 90−95.

https://doi.org/10.1021/acs.jpcc.4c08618
J. Phys. Chem. C 2025, 129, 7659−7666